

FeH Absorption in the Near-Infrared Spectra of Late M and L Dwarfs

Michael C. Cushing¹

Institute for Astronomy, University of Hawai‘i, 2680 Woodlawn Drive, Honolulu, HI 96822

cushing@ifa.hawaii.edu

John T. Rayner¹

Institute for Astronomy, University of Hawai‘i, 2680 Woodlawn Drive, Honolulu, HI 96822

rayner@irtf.hawaii.edu

Sumner P. Davis

Department of Physics, University of California, Berkeley, CA 94720

spdavis@physics.berkeley.edu

and

William D. Vacca¹

*Max-Planck-Institut fuer extraterrestrische Physik, Postfach 1312, D-85741 Garching,
Germany*

vacca@mpe.mpg.de

ABSTRACT

We present medium-resolution z -, J -, and H -band spectra of four late-type dwarfs with spectral types ranging from M8 to L7.5. In an attempt to determine the origin of numerous weak absorption features throughout their near-infrared spectra, and motivated by the recent tentative identification of the $E\ ^4\Pi - A\ ^4\Pi$ system of FeH near $1.6\ \mu\text{m}$ in umbral and cool star spectra, we have compared the dwarf spectra to a laboratory FeH emission spectrum. We have identified nearly

¹Visiting Astronomer at the Infrared Telescope Facility, which is operated by the University of Hawai‘i under contract from the National Aeronautics and Space Administration.

100 FeH absorption features in the z -, J -, and H -band spectra of the dwarfs. In particular, we have identified 34 features which dominate the appearance of the H -band spectra of the dwarfs and which appear in the laboratory FeH spectrum. Finally, all of the features are either weaker or absent in the spectrum of the L7.5 dwarf which is consistent with the weakening of the known FeH bandheads in the spectra of the latest L dwarfs.

Subject headings: molecular data—line:identification—infrared:stars—stars:low-mass,brown dwarfs

1. Introduction

Absorption bands due to FeH are ubiquitous in the red and near-infrared ($0.7 < \lambda < 1.3 \mu\text{m}$) spectra of late-type dwarfs. The most conspicuous FeH feature is the bandhead of the Wing-Ford band (Wing & Ford 1969) at $0.99 \mu\text{m}$ which arises from the $0-0$ ($v' - v''$) transition of the $F\ ^4\Delta - X\ ^4\Delta$ system. Schiavon et al. (1997) obtained moderate-resolution spectra ($R \sim 13,000$) of a sample of early to mid M stars to study the dependence of the Wing-Ford band on atmospheric parameters. Their spectra show that absorption features due to FeH dominate the spectra of the M dwarfs from 0.9850 to $1.0200 \mu\text{m}$. Other bandheads of this electronic system have also been detected in the spectra of late-type dwarfs including the $2-0$ at $0.7786 \mu\text{m}$ (Tinney & Reid 1998), the $1-0$ at $0.8692 \mu\text{m}$ (Kirkpatrick et al. 1999; Martín et al. 1999), the $2-1$ at $0.902 \mu\text{m}$ (Tinney & Reid 1998), the $0-1$ at $1.1939 \mu\text{m}$ (Jones et al. 1996; McLean et al. 2000; Leggett et al. 2001; Reid et al. 2001), and the $1-2$ at $1.2389 \mu\text{m}$ (McLean et al. 2000; Leggett et al. 2001; Reid et al. 2001).

In a recent study of infrared sunspot spectra, Wallace & Hinkle (2001, hereafter WH) identified 68 lines common to both a sunspot spectrum and a laboratory spectrum of FeH between 1.581 and $1.755 \mu\text{m}$. In addition, they identified four bandheads in the FeH spectrum at 1.58263 , 1.59118 , 1.62457 , and $1.61078 \mu\text{m}$. Based on the theoretical work of Langhoff & Bauschlicher (1990), they tentatively assigned this band to the $0-0$ transition of the $E\ ^4\Pi - A\ ^4\Pi$ system.

WH noted that three of the bandheads, at 1.58263 , 1.59118 , $1.62457 \mu\text{m}$, could be seen in the low-resolution spectra of late M and L dwarfs (e.g., Leggett et al. 2001). These bandheads probably account for the three unidentified absorption features in the spectra of L dwarfs at 1.58 , 1.613 , and $1.627 \mu\text{m}$ reported by Reid et al. (2001). WH also obtained a high-resolution ($R=50,000$), 70 \AA -wide spectrum of GJ 569B (M8.5 V) centered at $1.6578 \mu\text{m}$ and identified 13 lines common to both the dwarf spectrum and FeH spectrum. At least

in this narrow wavelength range, the dwarf spectrum was dominated by FeH absorption lines.

In the course of conducting a 0.8 to 4.2 μm spectroscopic survey of M, L and T dwarfs, we have identified numerous weak absorption features throughout the near-infrared spectra of the M and L dwarfs. In an attempt to determine the origin of these features, and motivated by the work of WH, we have compared our spectra to a laboratory FeH emission spectrum to determine whether FeH produces these absorption features.

In this paper, we present medium-resolution z -, J - and H -band spectra of four late-type dwarfs with spectral types ranging from M8 to L7.5 along with the identification of nearly 100 FeH absorption features. In §2, we discuss the dwarf spectra while in §3 we discuss the FeH spectrum. In §4 we compare the FeH spectrum and the dwarf spectra and in §5 we discuss our results. Our conclusions are summarized in §6.

2. M and L Dwarf Spectra

As part of a infrared spectroscopic survey of \sim 20 M, L, and T dwarfs, three of us (M.C.C., J.T.R., and W.D.V.) have obtained spectra of VB 10 (M8 V), 2MASS 1439+1929 (L1 V), 2MASS 1507–1627 (L5 V), and 2MASS 0825+2115 (L7.5 V) using SpeX (Rayner et al., in preparation) on the NASA Infrared Telescope Facility. The resolving power, R , of the spectra is \sim 2000 except for 2MASS 0825+2115 for which $R\sim$ 1200. The spectral classification of the L dwarfs is from Kirkpatrick et al. (1999). The observing strategy and data reduction techniques can be found in Cushing et al. (in preparation). The signal-to-noise of the spectra is >50 .

We use A0 V stars as telluric standards and as a result, care must be taken in removing the strong hydrogen absorption lines from their spectra. The standard procedure to remove intrinsic stellar lines is to interpolate across them using continuum points on either side of the lines. Although this process works well for isolated lines in regions where the atmospheric transmission is flat, it can introduce severe artifacts into the final spectra if performed in regions where there are many overlapping stellar lines and/or the atmospheric transmission is varying rapidly (Burgasser et al. 2002, Figure 3.14). Our telluric correction method (Vacca et al., in preparation) uses a high-resolution model spectrum of Vega to remove the intrinsic spectrum of the A0 V standards.

An example of the process is shown in Figure 1 which shows the H -band spectrum of the A0 V standard for VB 10 (lower spectrum), the resulting telluric correction spectrum (middle spectrum), and the theoretical atmospheric transmission for an airmass of 1.5 and 1.6 mm of

precipitable water vapor as computed with ATRAN (Lord 1992). We have also indicated the positions of the Brackett lines. Our telluric correction process removes the hydrogen lines in the A0 V star to a level of <2% above the continuum and leaves only the atmospheric transmission and instrument response function. The telluric correction spectrum is then divided into the dwarf spectra to remove telluric absorption and the instrument response function. The telluric correction process does not introduce artifacts into the dwarf spectra.

3. FeH Spectrum

One of us (S.P.D.) obtained the laboratory FeH spectrum using a King furnace at a temperature of 2700 K and the Fourier Transform Spectrometer at the McMath-Pierce Solar Telescope at Kitt Peak. The furnace sample was powdered iron and the filling gas was hydrogen at a pressure of 500 Torr. It is possible that water and other contaminants could produce additional absorption features in the resulting spectrum. To avoid this, an enclosed optical path was set up using large bore glass tubing that was flushed with flowing nitrogen. The spectrometer was set to a resolution width of 0.040 cm^{-1} which is equivalent to a resolving power $R \sim 150,000$ at $1.6 \mu\text{m}$.

A close examination of the spectrum from 0.96 to $2.00 \mu\text{m}$ verified that the lines analyzed by Phillips et al. (1987) were present, and accounted for all the strong emission lines between 0.78 and $1.34 \mu\text{m}$. Unidentified lines outside this region were assumed to be FeH because they showed the same line shapes and widths as those of identified lines. There were two regions of unidentified absorption lines in the spectrum, interspersed with the emission lines and centered at 1.13 and $1.95 \mu\text{m}$. None of the data in this paper covers regions that included absorption lines.

In the data-reduction process, the continuous background from the furnace was subtracted off, and the emission line spectrum set to a baseline of zero intensity. The observed line widths were twice the instrumental resolution width, owing somewhat to the high temperature but mostly to the high pressure of hydrogen. In order to compare the FeH spectrum to the dwarf spectra, we have degraded the resolution of the FeH spectrum to match that of the dwarf spectra by convolving it with a Gaussian of $\text{FWHM} = 5.4, 6.5, \text{ and } 8.1 \text{ \AA}$, the resolution of our observations in the z , J , and H bands, respectively.

4. Comparison of FeH and Dwarf Spectra

In the following sections, we compare z -, J -, and H -band spectra of the 4 dwarfs to the FeH spectrum. In addition to lowering the resolution of the FeH spectrum to $R=2000$ (see §2), we have resampled it onto the wavelength grid of the dwarf spectra. The vacuum wavelengths of the FeH features in the z , J , and H bands are given in Table 1. Since we cannot resolve individual FeH lines with a resolution of $R \sim 2000$, all of the the FeH features listed in Table 1 are blends of FeH lines.

4.1. z Band Comparison

Figure 2 shows the z -band spectrum of FeH and VB 10 in the lower and upper panels, respectively. The FeH absorption features in this spectral region arise primarily from the 0–0 band of the $F\ ^4\Delta - X\ ^4\Delta$ system. The strongest feature in the dwarf and FeH spectrum is the bandhead of the 0–0 band at $0.988\ \mu\text{m}$. We also have identified 33 absorption features redward of this bandhead which are present in the dwarf spectrum and in the FeH spectrum and have listed them in Table 1.

The feature at $1.0060\ \mu\text{m}$ arises from the the $F\ ^4\Delta_{7/2} - X\ ^4\Delta_{7/2}$ Q-branch (Phillips et al. 1987). Phillips et al. (1987) also identified another weaker Q-branch of the $(F\ ^4\Delta_{5/2} - X\ ^4\Delta_{5/2})$ at $0.997904\ \mu\text{m}$ which we cannot unambiguously identify. There are also three broad features in the VB 10 spectrum at 0.99513 , 1.03490 and $1.06664\ \mu\text{m}$ which have no counterparts in the FeH spectrum. The feature at $1.03490\ \mu\text{m}$ is most likely a blend of the Fe $a\ ^5\text{P}_2 - z\ ^5\text{F}_3^o$ line at $1.0343720\ \mu\text{m}$, the Ca $4p\ ^1\text{P}_1 - 5s\ ^1\text{S}_4$ line at $1.0346646\ \mu\text{m}$ and the two weak FeH features at 1.03398 and $1.03554\ \mu\text{m}$. This broad features disappears in the spectra of the mid L dwarfs revealing the two weaker FeH features. The other two features at 0.99513 and $1.06664\ \mu\text{m}$ remain unidentified because their shapes and relative strengths do not match the FeH features at those wavelength.

Figure 3 shows the z -band spectra of the four dwarfs. The 33 features are indicated with dotted lines. The bandhead, Q-branch, and 33 features are present in all of the dwarf spectra except for 2MASS 0825+2115 (L7.5 V) in which the features are either absent or considerably weaker. This dramatic weakening of the 0–0 band is consistent with the recent finding of Burgasser et al. (2002) and will be discussed in §5.

4.2. *J* Band Comparison

Figure 4 shows the *J*-band spectrum of FeH and VB 10 in the lower and upper panels, respectively. We believe the FeH features in this spectral region arise from the 0–1 and 1–2 bands of the $F\ ^4\Delta - X\ ^4\Delta$ system. The most prominent features are the bandheads of the 0–1 and 1–2 bands at 1.1939 and 1.2389 μm , respectively. There are also some atomic absorption features seen in the dwarf spectrum namely the K I $4p\ ^2\text{P} - 5s\ ^2\text{S}$ multiplet at 1.2432 and 1.2522 μm , the Al I $4s\ ^2\text{S} - 4p\ ^2\text{P}$ multiplet at 1.3117 and 1.3154 μm and the $a\ ^5\text{P}_3 - z\ ^5\text{D}_4^o$ Fe line at 1.1976 μm .

The features at 1.20907, 1.21126, 1.21348 and 1.22210 μm were previously identified as FeH absorption features by Jones et al. (1996). We have identified the feature at 1.22210 μm as the $F\ ^4\Delta_{7/2} - X\ ^4\Delta_{7/2}$ Q-branch (Phillips et al. 1987). In addition we have identified 24 new features which are present in the dwarf spectrum and in the FeH spectrum and have listed them in Table 1 along with the four features identified by Jones et al. (1996). The FeH features between 1.2 and 1.235 μm arise from the 0–1 band while the features longward of 1.24 μm arise from the 1–2 band although some P-branch lines from the 0–1 band are also present.

Figure 5 shows the *J*-band spectra of the four dwarfs. The 28 features are indicated with dotted lines. The bandheads, Q-branch, and 28 features are again present in all of the dwarf spectra except for 2MASS 0825+2115 (L7.5 V) where the features are either weaker or absent.

4.3. *H* Band Comparison

Figure 6 shows the *H*-band spectra of FeH and VB 10 in the lower and upper panels, respectively. We believe the absorption features in this spectral region are caused by FeH and arise from the 0–0 band of the $E\ ^4\Pi - A\ ^4\Pi$ system. Three of the four bandheads identified by Wallace & Hinkle (2001) at 1.58263, 1.59118, 1.62457 μm are clearly present. We have identified 34 features, 32 of which are new, that are present in the VB 10 spectrum and in the FeH spectrum and have listed them in Table 1. Two of the features at 1.65512 and 1.66100 μm are blends of the 13 FeH lines identified in the spectrum of GJ 569B by Wallace & Hinkle (2001). There is also a strong absorption feature at 1.64053 μm which has no counterpart in the FeH spectrum and remains unidentified. This feature is located within a much broader absorption feature which does appear in the FeH spectrum.

Figure 7 shows the *H*-band spectra of the 4 late-type dwarfs along with the location of the 34 features described above and three of the four bandheads identified by Wallace

& Hinkle (2001). The three bandheads and 34 features are conspicuous in all of the dwarf spectra except for 2MASS 0825+2115 (L7.5 V) where the FeH features are considerably weaker. This is consistent with the weakening of the FeH absorption features in both the z - and J -band and is further evidence that FeH is the cause of most of the absorption seen in the H -band spectra of late-type dwarfs.

5. Discussion

Our results indicate FeH is an important opacity source in the atmospheres of late-type dwarfs from 0.99 to 1.7 μm . Not only does FeH produce at least 6 bandheads in this wavelength range, but now nearly 100 weaker features which are presumably blends of numerous individual absorption lines. Although Wallace & Hinkle (2001) found that FeH absorption is present in the H -band spectra of late-type dwarfs, their detections were limited to the three bandheads and 13 lines in a narrow 70 \AA -wide spectrum. We have shown that medium-resolution dwarf spectra from 1.56 to 1.76 μm consist of numerous absorption features, almost all of which are due to FeH. Likewise, the 0.99 to 1.1 μm dwarf spectra consist of numerous absorption features which are also almost all caused by FeH.

As noted in §4, the FeH absorption features throughout the near-infrared spectra of 2MASS 0825+2115 (L7.5 V) are either much weaker than the earlier L dwarfs or absent entirely. Burgasser et al. (2002) have also found that the Wing-Ford band at 0.99 μm weakens and then disappears in mid to late L dwarfs. This is consistent with Fe condensing out of the atmosphere and forming a cloud layer which drops below the photosphere with decreasing effective temperature thus removing Fe-bearing molecules (FeH) from the layers above the cloud layer. However, they also find that the bandhead reappears in the early to mid T dwarfs. Since this is inconsistent with the scenario just described, Burgasser et al. (2002) propose holes are present in the cloud layer which allow the observer to see to deeper and thus hotter layers where FeH is not depleted. Unfortunately, we cannot test whether the FeH features in the J - and H -band spectra will reappear in early T dwarf spectra since strong methane absorption features appear in both the J - and H -band at these low effective temperatures and will mask any FeH features that may be present.

The appearance of two CrH bandheads of the $A\ ^6\Sigma^+ - X\ ^6\Sigma^+$ system at 0.86 (0–0) and 0.99685 (0–1) μm are a defining characteristic of the L spectral type. In fact, a spectral index based on the 0–0 bandhead is used to spectral type L dwarfs in the red-optical (Kirkpatrick et al. 1999). We question the identification of the 0–1 bandhead at 0.997 μm since there are three FeH absorption features at this wavelength that are apparent in the spectra of the mid M to late L dwarfs. This may explain the scatter in the spectral index defined using

the 0–1 bandhead (Kirkpatrick et al. 1999). Only higher resolution spectra will be able to determine to what extent the 0–1 CrH bandhead is present.

Finally, it should be noted that the opacities for FeH used in current atmospheric models are known to be incorrect (P. Bernath et al., in preparation). In addition, an analysis similar to that of Phillips et al. (1987) has yet to be performed on the new E $^4\Pi$ – A $^4\Pi$ system identified by Wallace & Hinkle (2001). Atmospheric models are necessary to determine the effective temperature scale for late-type dwarfs and until the correct FeH opacities are included in these models, obtaining good fits between the observations and models near FeH features may be difficult. Fortunately, there is work currently under way to revise the FeH opacities (P. Bernath et al., in preparation). Once this work is completed, it should also be possible to constrain the abundance of FeH in the atmospheres of late-type dwarfs as has recently be done for CrH (Burrows et al. 2002) and CO (Noll et al. 1997).

6. Conclusions

We have presented z -, J -, and H -band spectra of four dwarfs with spectral types ranging from M8 to L7.5. Using a laboratory FeH emission spectrum, we have identified nearly 100 FeH absorption features in the dwarf spectra. The H -band spectra contain 34 features which have counterparts in the FeH spectrum. Taken together with the results of Wallace & Hinkle (2001), our results suggest that FeH absorption dominates the spectra of late-type dwarfs from 1.56 to 1.76 μm .

M. Cushing acknowledges financial support from the NASA Infrared Telescope facility. We obtained the atmospheric transmission data from the Gemini Observatory, <http://www.gemini.edu/sciops>. We thank Sandy Leggett for useful discussions. This research has made use of the SIMBAD database, operated at CDS, Strasbourg, France as well as the Online Brown Dwarf Catalog (<http://ganymede.nmsu.edu/crom/cat.html>), which is compiled and maintained by Christopher R. Gelino at New Mexico State University. Finally we thank the referee, P. C. Stancil, for his useful suggestions.

REFERENCES

Burgasser, A. J., Marley, M. S., Ackerman, A. S., Saumon, D., Lodders, K., Dahn, C. C., Harris, H. C., & Kirkpatrick, J. D. 2002, *ApJ*, 571, L151

Burrows, A., Ram, R. S., Bernath, P., Sharp, C. M., & Milsom, J. A. 2002, *astro-ph* 0206159

Jones, H. R. A., Longmore, A. J., Allard, F., & Hauschildt, P. H. 1996, MNRAS, 280, 77

Kirkpatrick, J. D., Reid, I. N., Liebert, J., Curti, R. M., Nelson, B., Beichman, C. A., Dahn, C. C., Monet, D. G., Gizis, J. E., & Skrutskie, M. F. 1999, ApJ, 519, 802

Langhoff, S. R., & Bauschlicher, C. W. 1990, J. Mol. Spectrosc., 141, 243

Leggett, S. K., Allard, F., Geballe, T. R., Hauschildt, P. H., & Schweitzer, A. 2001, ApJ, 548, 908

Lord, S. D. 1992, NASA Technical Memor. 103957

Martín, E. L., Delfosse, X., Basri, G., Goldman, B., Forveille, T., & Zapatero Osorio, M. R. 1999, AJ, 118, 2466

McLean, I. S., Wilcox, K., M., Becklin, E. E., Figer, D. F., Gilbert, A. M., Graham, J., R., Larkin, J. E., Levenson, N., A., Teplitz, H., I., Kirkpatrick, J., D. 2000, 533, L45

Noll, K. S., Geballe, T. R., & Marley, M. S. 1997, ApJ, 489, L87

Phillips, J. G., Davis, S. P., Lindgren, B., & Balfour, W. J. 1987, ApJS, 65, 721

Reid, N. I., Burgasser, A. J., Cruz, K. L., Kirkpatrick, J. D., & Gizis, J. E. 2001, AJ, 121, 1710

Schiavon, R. P., Barbuy, B., & Singh, P. D. 1997, ApJ, 484, 499

Tinney, C. G., & Reid, I. N. 1998, MNRAS, 301, 1031

Wallace, L., & Hinkle, K. 2001, ApJ, 559, 424 (WH)

Wing, R. F., & Ford, W. K. 1969, PASP, 81, 527

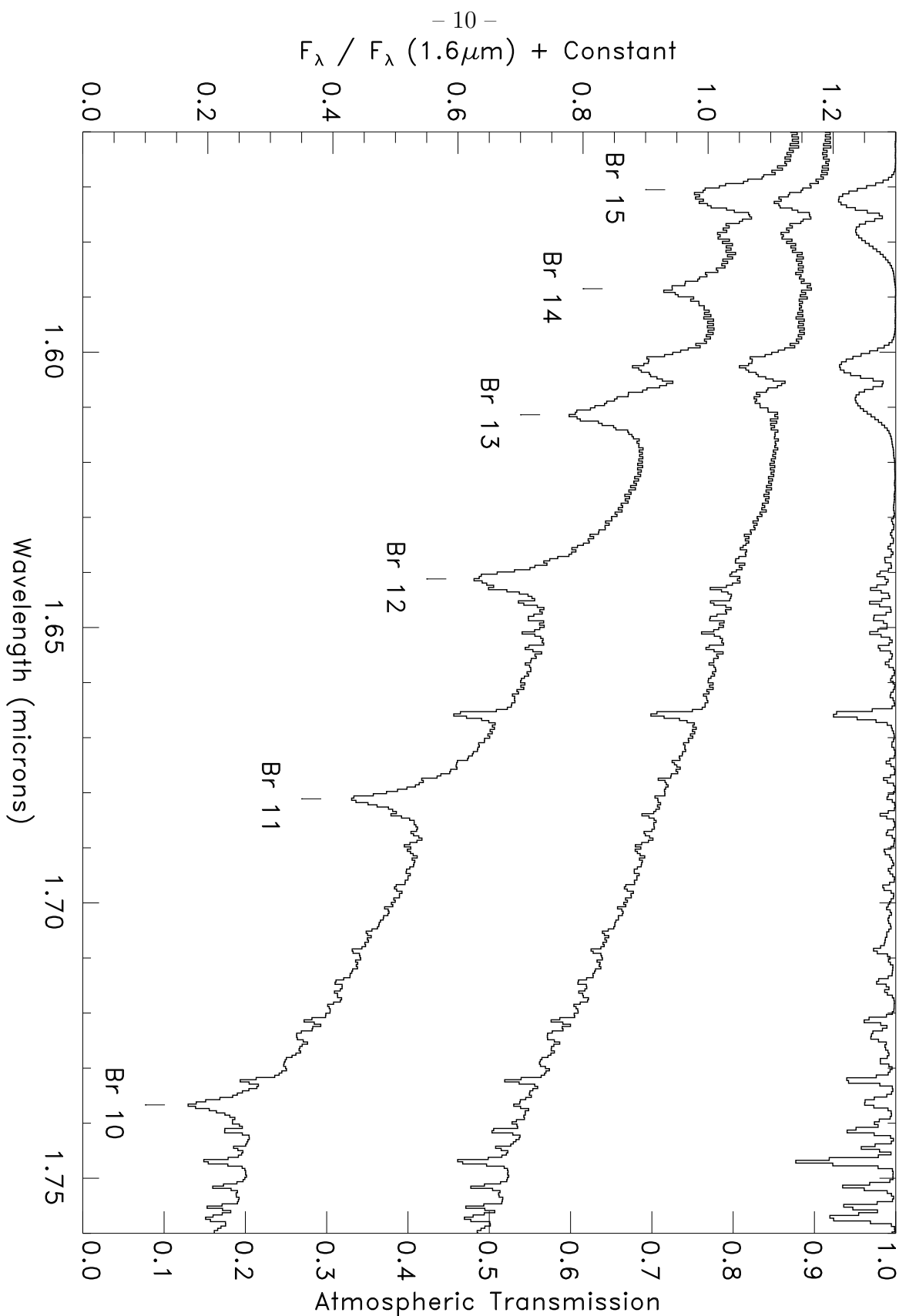


Fig. 1.— The lower spectrum is the observed A0 V standard, the middle spectrum is the telluric correction spectrum and the top spectrum is the theoretical atmospheric transmission. The positions of the Bracket lines are indicated.

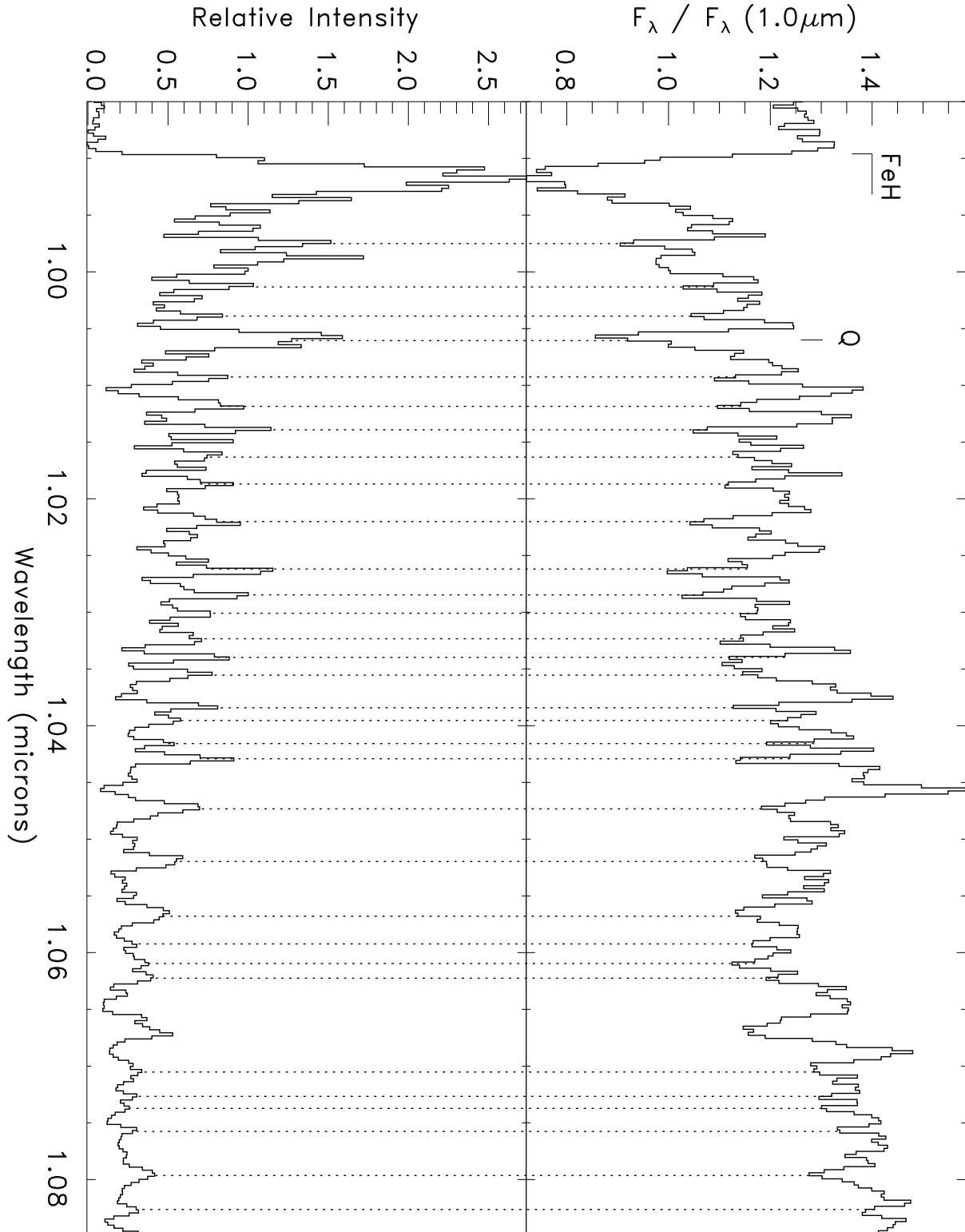


Fig. 2. ν_2 band: The lower panel is the FeH spectrum, and the upper panel is the VB 10 spectrum. The location of the 0-0 bandhead, and Q-branch are indicated. The 33 features are indicated with dotted lines.

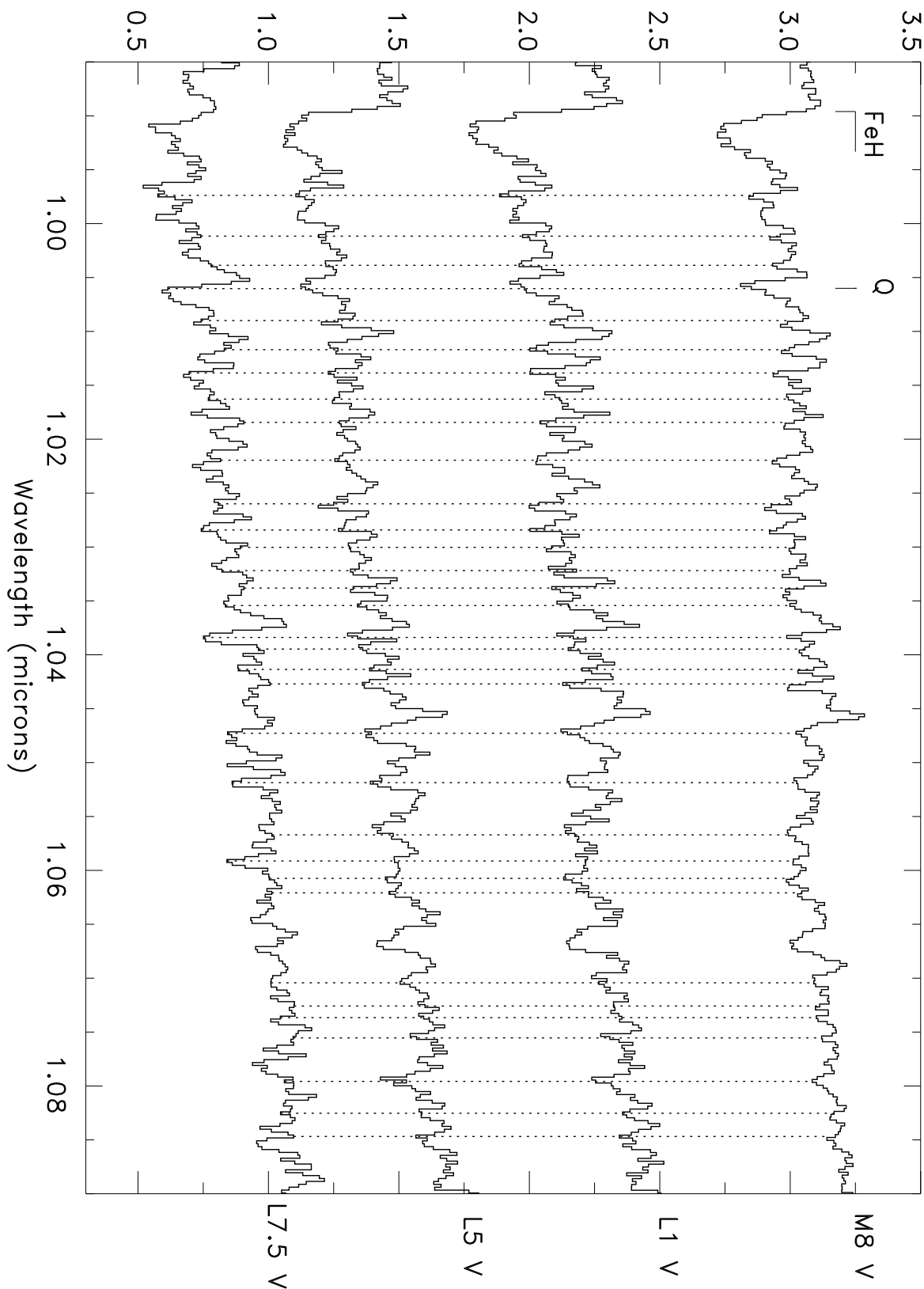


Fig. 3.— z band: The spectra of the 4 dwarfs. The location of the 33 features are shown with dotted lines as well as the bandhead and Q-branch feature.

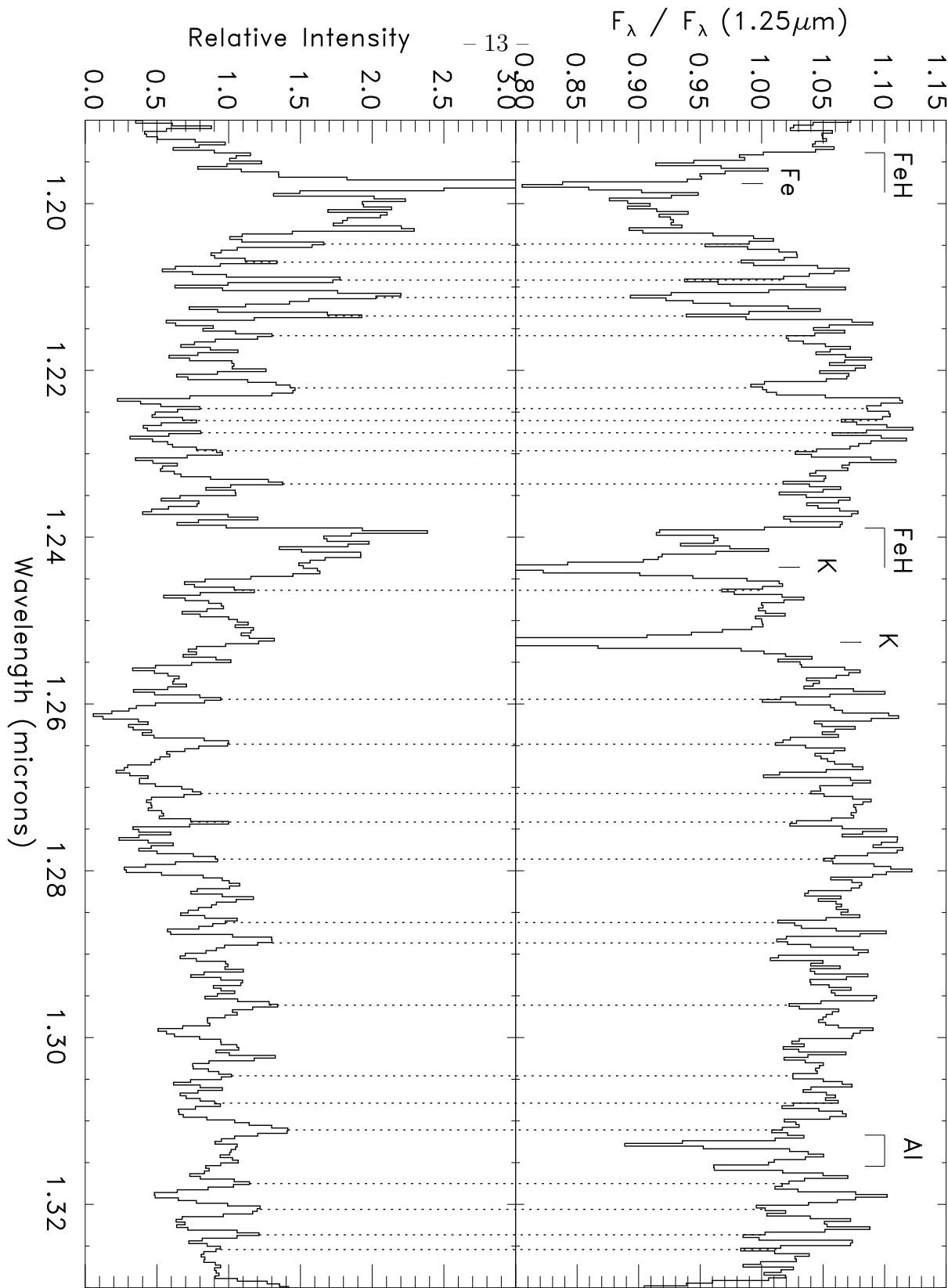


Fig. 4.— *J* band: The lower panel is the FeH spectrum and the upper panel is the VB 10 spectrum. The location K, Al, and Fe lines, as well as the 0–1 and 1–2 bandheads are indicated. The 28 features are indicated with dotted lines.

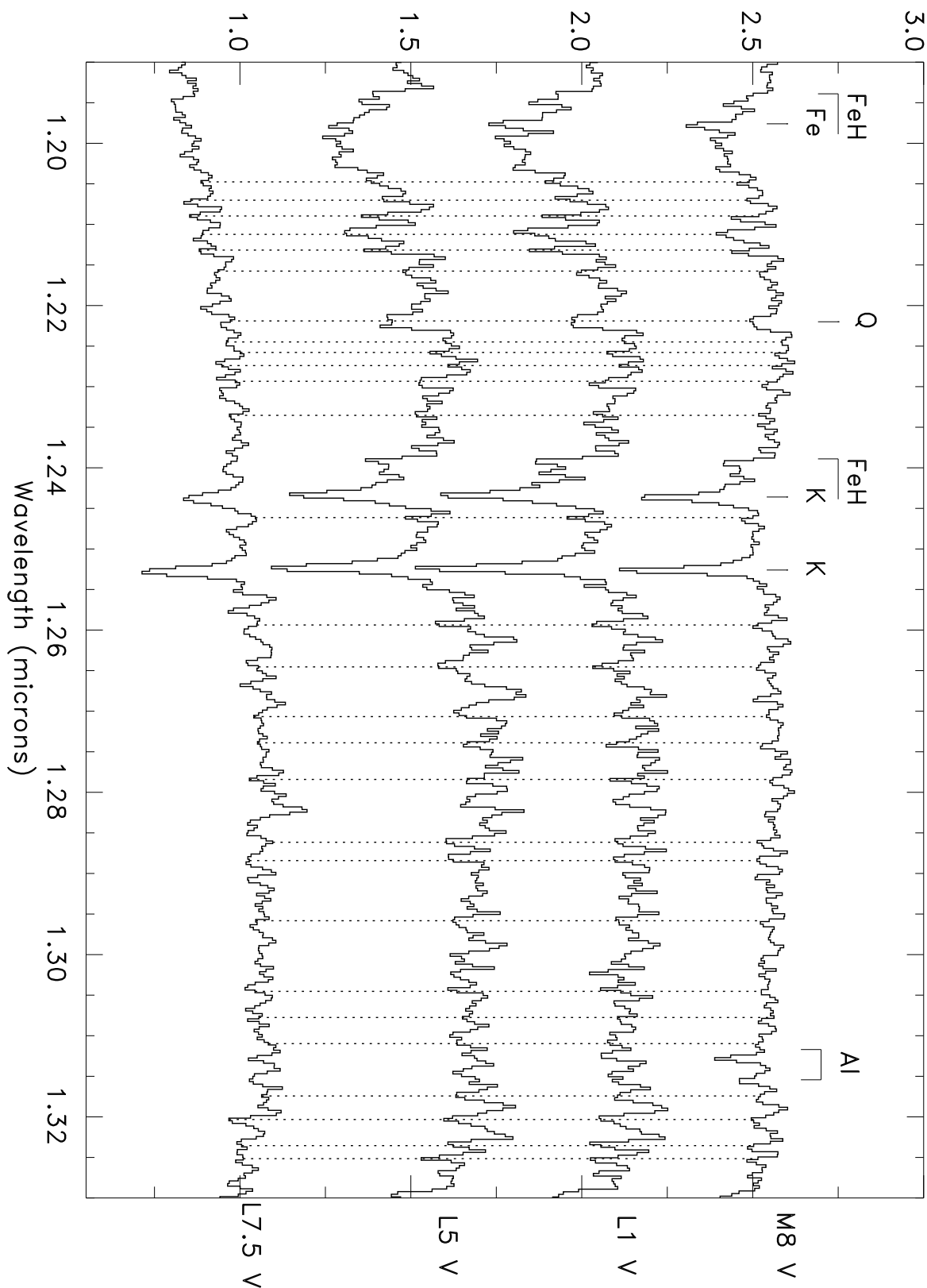
$$F_{\lambda} / F_{\lambda} (1.25\mu\text{m}) + \text{Constant}$$


Fig. 5.— *J* band: The spectra of the 4 dwarfs. The location of the 28 features are shown with dotted lines as well as the bandheads and Q-branch feature.

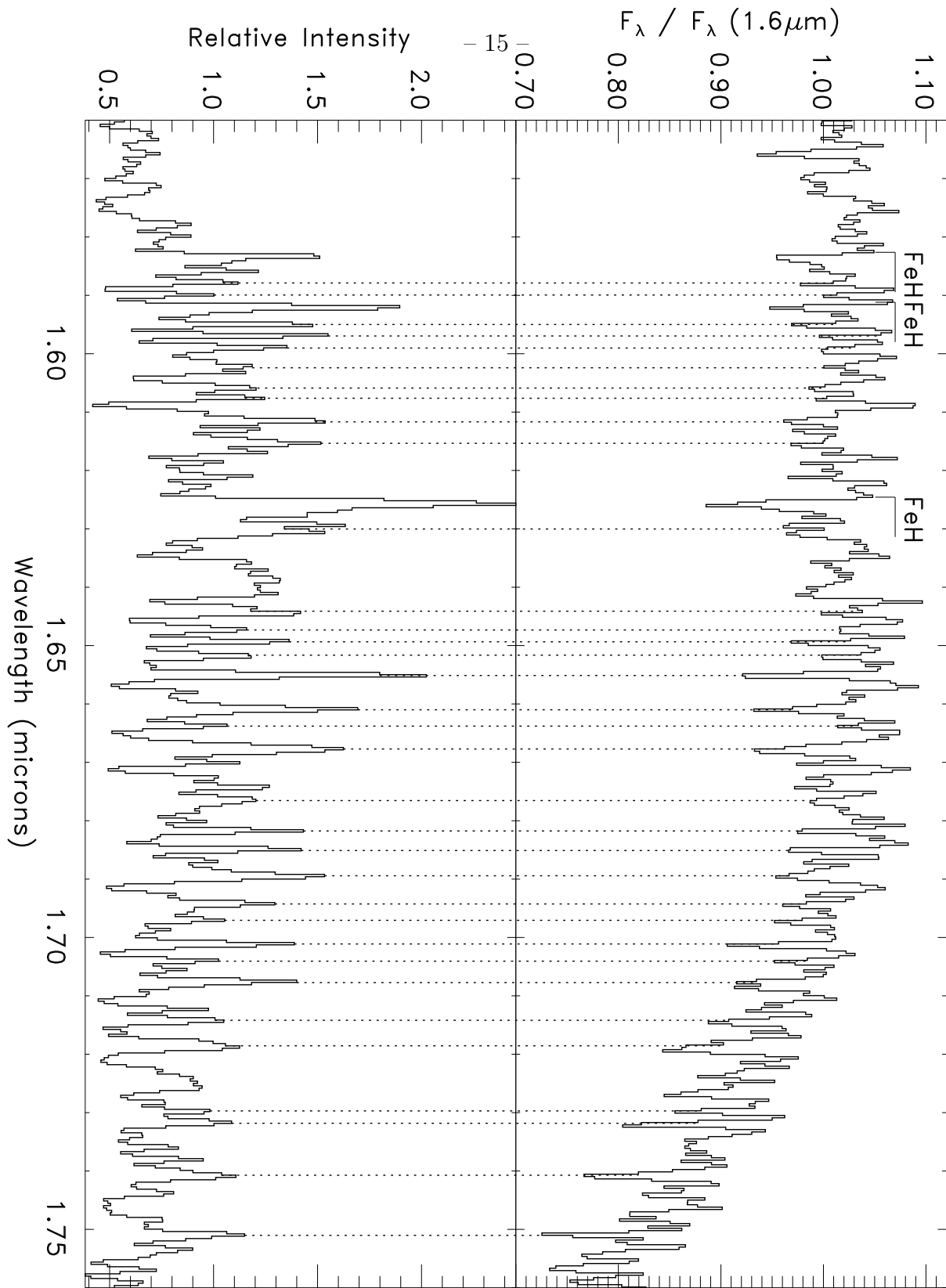


Fig. 6.— H band: The bottom panel is the FeH emission spectrum and the top panel is VB 10 spectrum. The location of the 34 features are indicated with dotted lines.

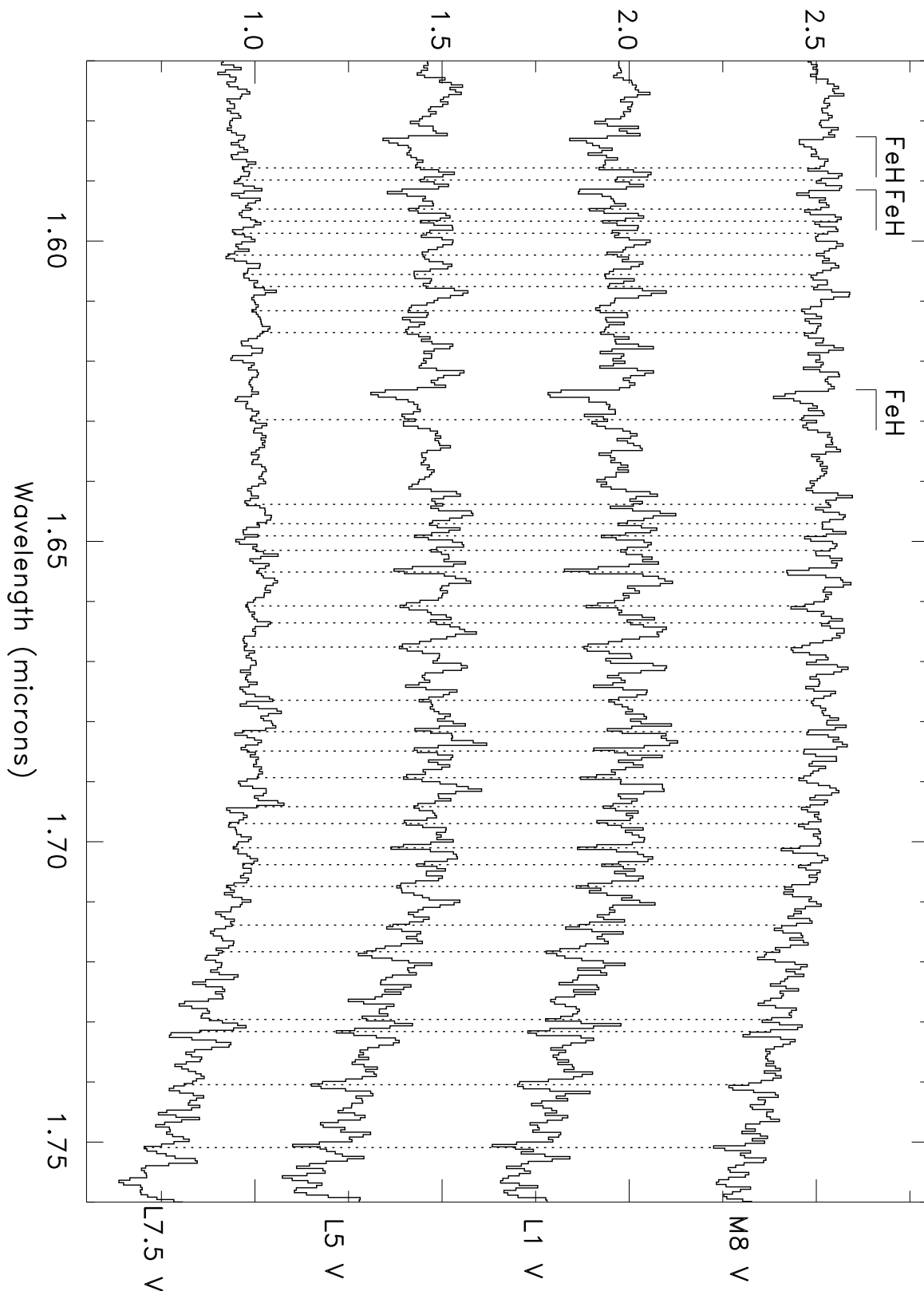
$$F_{\lambda} / F_{\lambda} (1.6 \mu\text{m}) + \text{Constant}$$


Fig. 7.— *H* band: The 1.56 to 1.76 μm spectra of the 4 dwarfs. The location of the 34 features are shown with dotted lines.

Table 1. Features Common to FeH and Dwarf Spectra

Vacuum Wavelength (μm)	Vacuum Wavelength (μm)	Vacuum Wavelength (μm)	Vacuum Wavelength (μm)
0.997510	1.06096	1.27074	1.64411
1.00133	1.06225	1.27416	1.64733
1.00390	1.07052	1.27860	1.64935
1.00606 ^a	1.07267	1.28621	1.65164
1.00926	1.07373	1.28866	1.65512
1.01185	1.07576	1.29612	1.66100
1.01392	1.07964	1.30459	1.66379
1.01633	1.08264	1.30786	1.66771
1.01870	1.08492	1.31108	1.67655
1.02201	1.20485	1.31751	1.68176
1.02619	1.20702	1.32060	1.68511
1.02847	1.20917	1.32365	1.68943
1.03009	1.21126	1.32542	1.69426
1.03234	1.21348	1.58788	1.69706
1.03398	1.21584	1.58995	1.70111
1.03554	1.22210 ^a	1.59499	1.70406
1.03842	1.22458	1.59696	1.70772
1.03954	1.22602	1.59903	1.71419
1.04157	1.22748	1.60241	1.71856
1.04291	1.22964	1.60588	1.72971
1.04733	1.23362	1.60763	1.73183
1.05197	1.24637	1.61167	1.74073
1.05679	1.25944	1.61535	1.75103
1.05923	1.26482	1.63002	

^aQ-branch